

# pH-Dependent Schemes of Calcium Carbonate Formation in the Presence of Alginates

Ashit Rao,<sup>†</sup> Patricio Vásquez-Quitral,<sup>‡</sup> María S. Fernández,<sup>‡</sup> John K. Berg,<sup>§</sup> Marianela Sánchez,<sup>‡</sup> Markus Drechsler,<sup>||</sup> Andrónico Neira-Carrillo,<sup>\*,‡</sup> José L. Arias,<sup>‡</sup> Denis Gebauer,<sup>†</sup> and Helmut Cölfen<sup>\*,†</sup>

<sup>†</sup>Department of Chemistry, University of Konstanz, Konstanz 78464, Germany

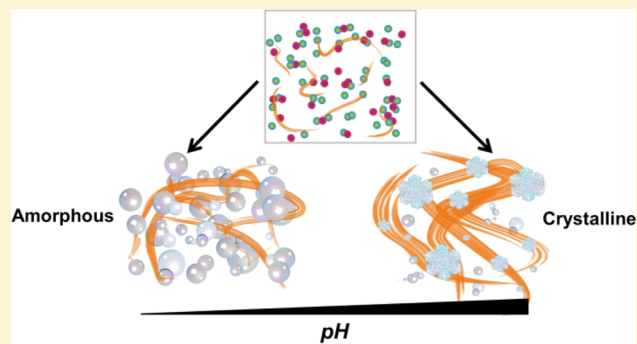
<sup>‡</sup>Faculty of Veterinary and Animal Sciences, University of Chile, Santiago, Chile

<sup>§</sup>Wood Materials Science, Institute for Building Materials, ETH Zürich, Zürich, Switzerland

<sup>||</sup>Maromolekulare Chemie II, University of Bayreuth, Bayreuth 95440, Germany

## Supporting Information

**ABSTRACT:** From recent studies on bone and shell formation, the importance of polysaccharides in biomineralization processes is gradually being recognized. Through ion-complexation and self-assembly properties, such macromolecules have remarkable effects on mineralization. However, their influences on the different regimes of crystallization including the interactions with precursor species are unclear. The present study therefore addresses calcium carbonate mineralization in the presence of alginates, a class of linear copolymeric saccharides composed of  $\beta$ -1,4 linked D-mannuronic and L-guluronic acid. During mineralization, this biopolymer is found to exert pH-dependent control over mineralization pathways in terms of the stability of prenucleation clusters, inhibitory effect toward nucleation and initially formed postnucleation products. Remarkably in the presence of this macromolecular additive, either amorphous or crystalline vaterite particles can be selectively nucleated in a pH-dependent manner. This is validated by electron microscopy wherein vaterite particles are intimately associated with alginate assemblies after nucleation at pH 9.75. At lower pH, aggregates of amorphous particles are formed. Thus, in addition to the general focus on biochemical properties of additives, solution pH, a physiologically fundamental parameter significantly alters the scheme of mineralization.



## INTRODUCTION

Biogenic minerals are the outcome of spatiotemporally regulated biophysical processes such as the transport of ions and biomolecules, stabilization of intermediate amorphous mineral precursors, and the deposition of organic–inorganic hybrid materials.<sup>1–5</sup> Several studies have focused on the role of proteins in these processes; however, polysaccharides have recently emerged to be important in the regulation of biomineralization.<sup>6</sup> For instance, proteoglycans such as chondroitin-, dermatan-, and keratan-sulfate regulate calcium carbonate ( $\text{CaCO}_3$ ) deposition in the crayfish gastrolith.<sup>6,7</sup> The growth of calcite during eggshell formation is concerted by dermatan sulfate on mammillae rich in keratan sulfate glycosaminoglycans.<sup>8,9</sup> Considering the physiologically relevant organic–inorganic interfaces in bone tissue, evidence shows direct association of mineral particles with proteoglycans.<sup>10</sup> Interestingly, sugar residues present as protein-associated glycan chains also prevent mineral-induced protein denaturation by sequestering ion species.<sup>11</sup> As the influence of certain carbohydrates over mineral deposition is gradually being understood, their fundamental roles in organic–inorganic interactions require elucidation.

Given the molecular diversity of carbohydrates, few studies have addressed their interactions with inorganic precursor species present during mineralization. Polysaccharide properties such as functional groups and degree of branching are known to affect crystal growth and morphology.<sup>12,13</sup> For example, a remarkable inhibitory effect is observed for calcite growth in the presence of amylopectin, a neutral polysaccharide.<sup>12</sup> Recently the role of mineral precursors such as prenucleation clusters<sup>14–18</sup> and amorphous phases<sup>19–22</sup> in mineralization has gained attention. To understand the effects of polysaccharides on the nascent stages of mineralization, diverse carbohydrates have also been assayed using a titration-based approach.<sup>23</sup> Seemingly minor properties such as molecular configuration, sugar stereochemistry, and type of glycosidic linkage have significant impacts on  $\text{CaCO}_3$  mineralization. For example, L-glucose has a stabilizing effect toward prenucleation clusters, in contrast to its stereoisomer, D-glucose, which has no significant stabilizing effect. Maltose and trehalose, dimers of D-

Received: October 20, 2015

Revised: January 7, 2016

Published: February 9, 2016

glucose that differ in the nature of glycosidic linkages, exhibit contrasting effects toward prenucleation cluster stability. In light of these observations, detailed investigations addressing the fundamental interactions between carbohydrates and mineral species are required. The present study therefore investigates the effects of alginates on the early stages of  $\text{CaCO}_3$  mineralization.

Alginates are linear copolymer polysaccharides composed of  $\beta$ -1,4 linked D-mannuronic (M) and L-guluronic (G) acids present in certain algae.<sup>24</sup> The M and G units are arranged in a block-wise manner with homopolymeric M and G blocks interspaced with alternating MG blocks.<sup>25</sup> Species dependent variations in the ratio and sequence of the M and G units<sup>26</sup> determine the emergent physical properties.<sup>27</sup> Alginates are relevant to mineralization because the G units can interact with divalent cations such as  $\text{Ca}^{2+}$  and  $\text{Ba}^{2+}$  among others by “egg-box” binding motifs.<sup>28–30</sup> At sufficiently high ion concentrations, these biopolymers form stable hydrogels via multiple steps viz. ion complexation, dimerization, and lateral association of the biomolecules with helical conformations.<sup>31,32</sup> It is known that hydrogels play an important role in biomineralization like for example silk hydrogels in the formation of nacre,<sup>33</sup> but also in bioinspired mineralization, hydrogels can play a crucial role as demonstrated for agarose hydrogels.<sup>34</sup> Therefore, the investigation of hydrogel forming polysaccharides like alginates and their influence on mineralization is especially interesting.

Several investigations using alginates report interesting effects on crystal growth. These additives modulate crystal growth by leading to rounded morphologies uncharacteristic of rhombohedral calcite grown in gas diffusion experiments.<sup>35</sup> Typically, alginate induces the formation of vaterite that gradually transforms to large calcite particles.<sup>36</sup> Applying mineralization conditions with crystal seeds, alginates inhibit vaterite growth and lead to extensive agglomeration.<sup>36</sup> These studies imply a high affinity of alginate molecules for vaterite. Thus, previous investigations have addressed the products of mineralization in terms of shape and polymorph composition. Certain synthetic polymers such as double-hydrophilic block copolymeric surfactants also have remarkable effects on  $\text{CaCO}_3$  crystal formation and morphology.<sup>37–40</sup> Lately, the role of prenucleation clusters in mineralization is emerging to be significant in different mineral systems including calcium phosphates, calcium carbonates, and iron(oxy) (hydr)oxides.<sup>15,16,18,23,41,42</sup> The structure and stability of such mineral precursor species as well as the chemical nature of additives have profound influences on the properties of postnucleation products including polymorph selection, superstructure formation, and nucleation inhibition.<sup>23,42–44</sup> Hence to understand the effects of biomolecules on mineral formation, techniques to quantitatively probe events associated with prenucleation and early nucleation regimes of mineralization are required.

In this work, commercial alginates and alginates isolated from brown algae (*Lessonia trabeculata* and *Lessonia nigrescens*) are investigated for their effects on the different stages of  $\text{CaCO}_3$  crystallization. Potentiometric titration is applied to provide quantitative information on nucleation events in bulk volumes under fine-tuned experimental conditions.<sup>18</sup> Prenucleation cluster (PNC) species and other mineral precursors are particularly sensitive to parameters such as pH, temperature, and ionic strength,<sup>18,45–47</sup> further validating the use of this method. Remarkably, the effects of the alginate additives on mineralization vary significantly in a pH-dependent manner. Experiments using electron microscopy including scanning and

transmission electron microscopy (TEM) and cryo-TEM are performed to validate these results. Similar observations for the individually tested alginate additives indicate that solution pH is an important determinant for interactions between additives and PNCs as well as the fate of transient mineralization precursors.

## ■ EXPERIMENTAL SECTION

**Chemicals.** Milli-Q (EMD Millipore Inc., Billerica, MA USA) water was used in all experiments unless specified otherwise. Calcium chloride ( $\text{CaCl}_2$ , Fluka, 1 M volumetric solution) and sodium hydroxide (NaOH, Alfa Aesar, 0.01 M standard solution) were used for titration assays. Commercial low and medium viscosity alginic acids (CAS 9005-38-3) were purchased from Sigma-Aldrich.

**Preparation of Alginates.** Commercial alginates (5 g) were dissolved in deionized distilled water (1 L) and filtered using Whatman filter paper (No. 1 and No. 42). The filtrate was precipitated using cold ethanol at a final concentration of 70% v/v. The precipitate was washed twice with absolute ethanol. Then the alginate was dried at 45 °C for 24 h, followed by incubation in a desiccator at r.t. for 24 h, and refrigerated until further use. Purification of alginates from *L. nigrescens* and *L. trabeculata* was done by following an acid precipitation protocol described previously.<sup>48</sup>

**Analytical Ultracentrifugation.** Sedimentation velocity experiments were performed using a Beckman XL-I ultracentrifuge (Beckman Coulter Inc., Palo Alto, CA USA) using interference optics and 12 mm titanium double sector cells (Nanolytics) at 25 °C. The sedimentation velocity data were analyzed using the software program SEDFIT version 9.4 (P. Schuck, NIH, Bethesda, Md USA) to generate sedimentation coefficient distributions.<sup>49</sup>

**Potentiometric Titrations.** Potentiometric titration experiments were performed by using a titration system (Metrohm GmbH, Filderstadt, Germany) operated using a software (Tiamo v2.2, Metrohm GmbH, Germany). During these measurements, the pH and free  $\text{Ca}^{2+}$  concentrations were monitored by a flat membrane glass electrode and a polymer-based ion-selective electrode, respectively.  $\text{CaCl}_2$  (10 mM) solution was dosed at a constant rate of 0.01 mL/min to alginate dissolved in carbonate buffer (10 mM, 20 mL), under constant stirring at 800 rpm. A constant pH was maintained by automatic counter-titration of NaOH (10 mM). Calibration and reference experiments were performed by dosing  $\text{CaCl}_2$  (10 mM) into water and carbonate buffer (10 mM, 20 mL) at different pH values. These experiments were comprehensively described in the previous literature.<sup>14,18,45,50</sup> To investigate the effects of alginates on mineral growth, titrations were stopped at nucleation and quenched using absolute ethanol.<sup>51</sup> After centrifugation, the pellets obtained were washed with absolute ethanol and vacuum-dried in a Vacuum Concentrator Plus (Eppendorf).

**Transmission Electron Microscopy.** Samples drawn from titration experiments were deposited on a TEM grid (Cu, Formvar coated; Ted Pella, Inc., CA USA). A Libra 120 (Zeiss SMT GmbH, Germany) TEM operated at an acceleration voltage of 120 kV with a beam current of 4  $\mu\text{A}$  was used for imaging.

**Fourier Transformed Infrared Spectroscopy (FTIR).** FTIR analysis of the quenched samples is done using a PerkinElmer Spectrum100 spectrometer using an attenuated total reflection (ATR) configuration.

**Scanning Electron Microscopy (SEM).** SEM analysis was performed using a desktop Hitachi TM-3000 (Hitachi High-Technologies Europe GmbH, Germany) equipped with an energy dispersive detector.

**Cryo-Transmission Electron Microscopy (Cryo-TEM).** During the course of titration measurements, samples were prepared by blotting the drop onto a thin film on a lacey carbon film covered copper grid and vitrified by liquid ethane at its freezing point (90 K) by means of a cryo-box (Carl Zeiss Microscopy, Germany). The vitrified specimens were loaded into a cryo-holder and examined in a LEO EM922Omega EFTEM (Carl Zeiss Microscopy, Germany).

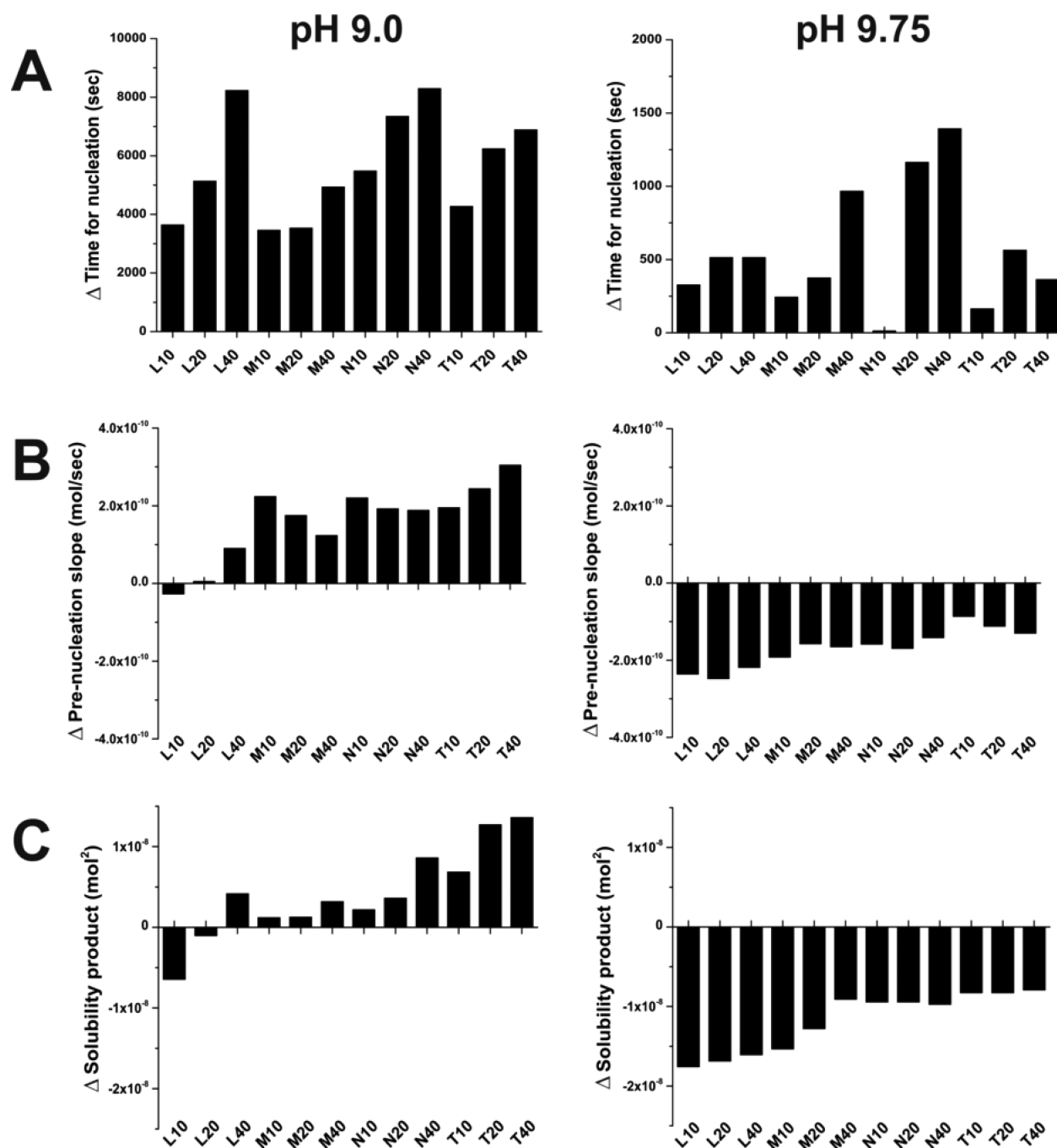


**Figure 1.** Bar plots representing the effects of alginates in terms of changes to the (A) time required for nucleation, (B) prenucleation slope, and (C) solubility of initially nucleated phase in comparison with reference titrations at pH 9.0 and 9.75. The  $x$ -axis represents four alginates (commercial low viscosity, L; medium viscosity, M; and those isolated from *L. nigrescens*, N; *L. trabeculata*, T) at 10, 20, and 40 mg/L.

Images were recorded with a high-resolution, cooled CCD camera using the Gatan Digital Micrograph software package.

**Gas Diffusion Assay.** Crystallization experiments were performed in the presence of alginates using gas diffusion, the details of which are described previously.<sup>52</sup> Control experiments were performed in absence of alginates. The  $\text{CaCO}_3$  crystals thus obtained were rinsed with Milli-Q water, dehydrated with growing concentration of ethanol from 50% to 100%, and finally dried at room temperature. The samples were analyzed using SEM.

## RESULTS AND DISCUSSION

**Investigating Mineral Nucleation in the Presence of Alginates.** Potentiometric titration is an ideal technique to

quantitatively probe the effects of additives on the early stages of mineralization<sup>9,23</sup>. These experiments help to elucidate the formation and structure of PNCs and their subsequent effects on nucleation. By using small biomolecules as mineralization additives during titration, properties such as stereochemistry, polarity, the presence of  $\text{Ca}^{2+}$  binding sites, and the type of glycosidic linkages are found to significantly affect mineralization.<sup>11</sup> More complex biomacromolecules such as sea urchin and nacre-derived proteins also have distinct effects on the early stages of  $\text{CaCO}_3$  formation.<sup>32</sup> In addition, the applications of this technique in understanding other mineralization systems as well as quantitatively assessing anti-scalants and other additives

underscore its merits in studying nucleation phenomena.<sup>15,16,42,53–58</sup>

In the present study, potentiometric titrations are used to analyze the interactions between the alginates and ions/prenucleation clusters, inhibitory effects toward nucleation, and the initial products formed postnucleation. The sedimentation coefficient distributions for the four alginate samples investigated here present single peaks indicating homogeneous sample compositions of comparable molar mass distributions (Figure S1 and Table S1). Titrations containing different alginate contents are conducted at constant pH values of 9.0 and 9.75. Plots illustrating the development of free  $\text{Ca}^{2+}$  ions and solubility products are presented in the Supporting Information (Figures S2–S5). The data are summarized as bar plots representing the differences between alginate-containing and reference titrations (Figure 1). The time periods required for initial nucleation of a solid mineral phase in the presence of alginates are summarized in Figure 1A. Here we apply a scaling factor  $F$ , the quotient of the nucleation times in the presence and absence of an additive to compare inhibitory effects toward nucleation.<sup>23,53</sup>  $F$  values lower or greater than unity indicate the tendency of additives to promote or inhibit nucleation, respectively. A more pronounced inhibition toward nucleation is clearly evident at pH 9.0 wherein an average  $F$  value of  $1.85 \pm 0.2$  is observed in comparison to a corresponding value of  $1.19 \pm 0.1$  at pH 9.75 (estimated for nucleation times in titrations with 40 mg/L alginate). At pH 9.0, the general trend is that the inhibition increases with the alginate concentration, but this trend is not found at pH 9.75. Complexation of  $\text{Ca}^{2+}$  ions is indicated by minor offsets in the development of free ion concentration during the prenucleation regimes for titration at both pH values. However, considering the distinct pH-dependent inhibitory effects of the additives,  $\text{Ca}^{2+}$  ion complexation alone cannot explain this behavior. The  $\text{pK}_a$  of carboxylate groups in the sugar residues comprising alginate chains is about 3.5. Hence these groups would be predominantly anionic and expected to not exhibit a significant variation in the deprotonated form for carboxylate groups at pH 9.0 and 9.75. These observations indicate that the inhibition of nucleation in the presence of additives cannot be solely attributed to ion complexation. Previous studies indicate that the interactions of additives with precursor mineral species such as PNCs can modulate the time needed for nucleation. For example, the stoichiometry of  $\text{Ca}^{2+}$  binding in the presence of poly(acrylic acid) does not completely account for its inhibitory effect toward  $\text{CaCO}_3$  nucleation.<sup>42</sup> Further evidence comes from the delay of nucleation induced by amino acids such as glycine, serine, and methionine as well as certain saccharides including D-ribose, which are small molecules with poor ion-complexation properties.<sup>23</sup> Although the physical interactions at the molecular scale leading to these distinct effects are unclear, pH related factors such as the ratio of carbonate-bicarbonate ions and proto-structures of mineral precursors can affect the interactions between additives and mineral precursors.<sup>18,51</sup> In addition to solution pH being a factor affecting nucleation time, the inhibitory behavior of alginates is also dependent on additive concentration. For example, 10 and 40 mg/L low viscosity commercial alginate lead to respective  $F$  values of 1.4 and 2.0 at pH 9.0. Similar trends are observed in the presence of other alginate additives.

The slope of the prenucleation regime in plots of free  $\text{Ca}^{2+}$  ion concentrations reflects the interactions between additive

molecules and solute ion associates, i.e., PNCs.<sup>18,42</sup> A steeper slope in comparison to reference experiments indicates an equilibrium shift toward free ions and less bound calcium, whereas a lower slope reflects cluster stabilization effects induced by additives.<sup>16,18,42</sup> The values of this parameter in the presence of alginates are presented in Figure 1B. The pH-dependent effects on the prenucleation regime are distinct. At pH 9.0, most alginates exhibit a destabilizing effect toward  $\text{CaCO}_3$  PNCs. Highest destabilization of clusters is induced by *L. trabeculata* alginate reflected by a 60% increase in the slope relative to reference experiments, whereas low viscosity alginate induced cluster destabilization at pH 9.0 is less pronounced. Thus, molecular properties such as molar mass, ratio, and sequence of the M and G units as well as self-assembly states<sup>59</sup> appear to affect the thermodynamic stability of ion clusters. At higher pH, the prenucleation regimes display lower slope for all alginates in comparison to reference experiments. These biomolecules induce stabilization of PNCs in remarkable contrast to their effects at pH 9.0 (Figure 2). At pH 9.75, the

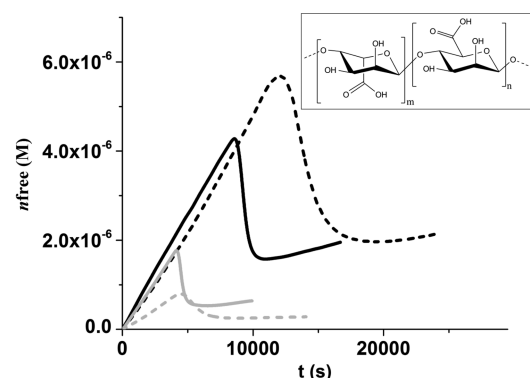


**Figure 2.** Development of free  $\text{Ca}^{2+}$  ions with time at pH 9.0 (black) and pH 9.75 (gray) in reference (continuous line) and low viscosity alginate (dashed line) containing titrations. Inset shows a representation of the linear structure of alginate with  $\beta$ -D-mannuronic acid (M) and  $\alpha$ -L-guluronic acid (G) residues with  $\beta$ -1,4 linkages.

decrease in the prenucleation slope is highest in the presence of low viscosity alginate. Medium viscosity alginates and the alginates isolated from *Lessonia* species induce intermediate effects toward the decrease in the prenucleation slope. Previous studies show that molecular properties of sugar residues can significantly affect the early stages of mineralization.<sup>23</sup> However, the changes in such molecular factors are generally insignificant between pH 9.0 and 9.75. Bearing in mind the inorganic phase, transient mineral species are significantly affected by solution pH.<sup>51</sup> It emerges that the nature of organic interfaces with nascent mineral precursor species is crucial in determining the early mineralization events. However, investigating the interactions between additives and transient mineral precursors is challenging because of the transient nature of amorphous phases as well as their sensitivity to experimental conditions such as pH, temperature, ionic strength, solvents, and electron irradiation.<sup>15,50,51,60,61</sup>

Recent evidence suggests that the pH-dependent stabilities of PNCs can affect subsequently formed phases after nucleation.<sup>18,19</sup> It follows that additives which affect the slope of the prenucleation regime also influence the solubility products of the initially nucleated phases, i.e., regulate polymorphism.<sup>16,23,42</sup> In this study, alginates induce a pH related destabilizing or stabilizing effect on  $\text{CaCO}_3$  PNCs (Figure 1C). This also has a

corresponding influence on the polymorph of CaCO<sub>3</sub> initially nucleated. In agreement with previous literature, reference titrations yield values of solubility products  $3.1 \times 10^{-8}$  and  $3.8 \times 10^{-8} \text{ M}^2$  at pH 9.0 and 9.75, respectively.<sup>18</sup> With alginates at pH 9.0, the solubility products of the initially nucleated phase are in the range of  $3 \times 10^{-8}$  and  $4.5 \times 10^{-8} \text{ M}^2$ . These values indicate the formation of amorphous CaCO<sub>3</sub> (ACC) phases after nucleation. An exception is the nucleation of vaterite ( $1.8 \times 10^{-8} \text{ M}^2$ ) in the presence of 10 mg/L low viscosity alginate. However, this is also consistent with a decrease in the corresponding prenucleation slope. At pH 9.75, the additives induce formation of vaterite, a crystalline form a CaCO<sub>3</sub> after nucleation. The corresponding postnucleation products of solubility are between  $2.0 \times 10^{-8}$  and  $2.9 \times 10^{-8} \text{ M}^2$  and are considerably lower than that of ACC.<sup>9</sup> Note that similar effects are observed for all alginate additives at pH 9.75. This validates the notion that more stable PNCs nucleate solid phases that have higher stability,<sup>19</sup> although it appears that the solubility of the ACC intermediate that occurs under these conditions (see below) cannot be quantified owing to its transient character. To better understand the distinct mineralization schemes at different pH values and the interactions between biomolecules and mineral precursors, electron microscopy experiments are performed for titration products in the presence of low viscosity alginates.

**Analyzing the pH Dependence of Nucleation Behavior.** Initial analyses of the titration products obtained at pH 9.0 and 9.75 are done using SEM (Figure 3). At low magnification,

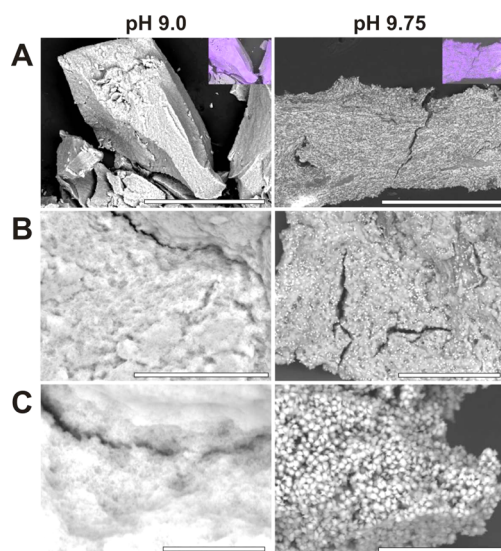


**Figure 3.** SEM images of products nucleated from titrations containing 40 mg/L low viscosity commercial alginate at pH 9.0 and 9.75. Scale bars represent (A) 500, (B) 100, and (C) 20  $\mu\text{m}$ . Insets in row (A) represent EDS derived calcium localization (purple) maps.

the particles precipitated at pH 9.0 exhibit uniform contrast. In comparison, fibrous aggregates with granular appearance and areas distinct in contrast are observed at pH 9.75. Energy-dispersive X-ray spectroscopy indicates overall similar contents of calcium, carbon, and oxygen in these samples (Figure S6). However, elemental mapping shows local sites with significantly higher calcium content for samples nucleated at pH 9.75 (Figure S7). At higher magnification, the structural features are more distinct (Figure 3B,C). Low-viscosity alginate-containing titrations conducted at pH 9.0 show continuous, coarse surfaces

indicative of porosity. On the other hand, calcium-rich mineral particles are associated with the alginate aggregates at pH 9.75. These lens-like particles are previously reported for alginate-containing gas diffusion experiments.<sup>62</sup> SEM and TEM images of alginate samples in the absence of mineralization show distinct structures with a nano- and microporous nature (Figure S8). To further investigate the sample compositions, FTIR spectra are measured after solvent-exchange mediated quenching for the stabilization of possible amorphous phases. The FTIR spectra for samples from titrations conducted at pH 9.0 and 9.75 are presented in Figure S9. In the presence of alginates (40 mg/L) at pH 9.0, a significant band characteristic of ACC ( $\nu_2$ ) is observed at  $862 \text{ cm}^{-1}$ . Bands at  $1075$  and  $725 \text{ cm}^{-1}$  also correspond to the  $\nu_1$  and  $\nu_4$  vibrational modes of proto-structured pc-ACC.<sup>29</sup> Similar spectra are observed for reference experiments conducted at pH 9.0. At pH 9.75, the spectra for alginate containing and reference samples significantly differ. The reference spectra exhibit bands at  $721$ ,  $864$ , and  $1072 \text{ cm}^{-1}$  typical of ACC. This is consistent with previous literature.<sup>51</sup> However, the FTIR spectra of samples prepared in the presence of alginates at pH 9.75 indicate significant deviation in the mineral composition. Bands present at  $744$  ( $\nu_4$ ),  $871$  ( $\nu_2$ ), and  $1085$  ( $\nu_1$ )  $\text{cm}^{-1}$  validate the formation of vaterite, consistent with the results of potentiometric titration assays. Thus, alginates promote the formation of crystalline CaCO<sub>3</sub> at higher pH values.

The interactions between alginates and inorganic species at the submicron length scales are investigated using TEM. Analyses of samples from titrations at pH 9.0 indicate aggregates of particles that are polydisperse, about 30–100 nm in size (Figure 4A–C). SAED patterns indicate the amorphous nature of the aggregates. Amorphous fibril-like structures may correspond to alginate assemblies (arrow, Figure 4C). At pH 9.75, particles with high contrast are observed in association with a fibrillar network of alginates (Figure 4D). These particles show two distinct regions having a dense structure ( $\sim 1 \mu\text{m}$  in size) surrounded by smaller nanoparticles ( $\sim 40 \text{ nm}$ ). The SAED pattern corresponding to the compact regions is typical of single crystalline vaterite with reflections at  $d$  values at 3.34, 2.75, 2.34, and 1.88 Å corresponding to {113}, {116}, {122}, and {036} faces (Figure 4F). The nanoparticles in proximity of the vateritic structures however are amorphous. The evasion of this phase in potentiometric titration and FTIR spectra indicates its short-lived nature and a possible role as a precursor to crystalline CaCO<sub>3</sub>, vaterite. The nature of mineral products from reference and alginate-containing solutions is consistent with the titration experiments considering the initially nucleated phases at respective pH values. To avoid artifacts due to sample drying, cryo-TEM experiments were performed.

Samples drawn during the progression of titration experiments at pH 9.75 were analyzed using cryo-TEM (Figure 5). During the early prenucleation stage (Figure 5A,B) aggregates that gradually increase in contrast over time were observed. This indicates assembly of alginates and possible colocalization of inorganic precursor species during the early stage of CaCO<sub>3</sub> nucleation. Densification of the aggregates and initial growth of mineral particles were seen during the nucleation event (Figure 5C,D). The nucleation regime distinctly affects the assembly of alginates to more structured fibrillar and sheet-like morphologies (Figure S10). Subsequent to nucleation, the growth of superstructures formed of smaller particles was observed (arrows, Figure 5E,F). The SAED pattern of these structures

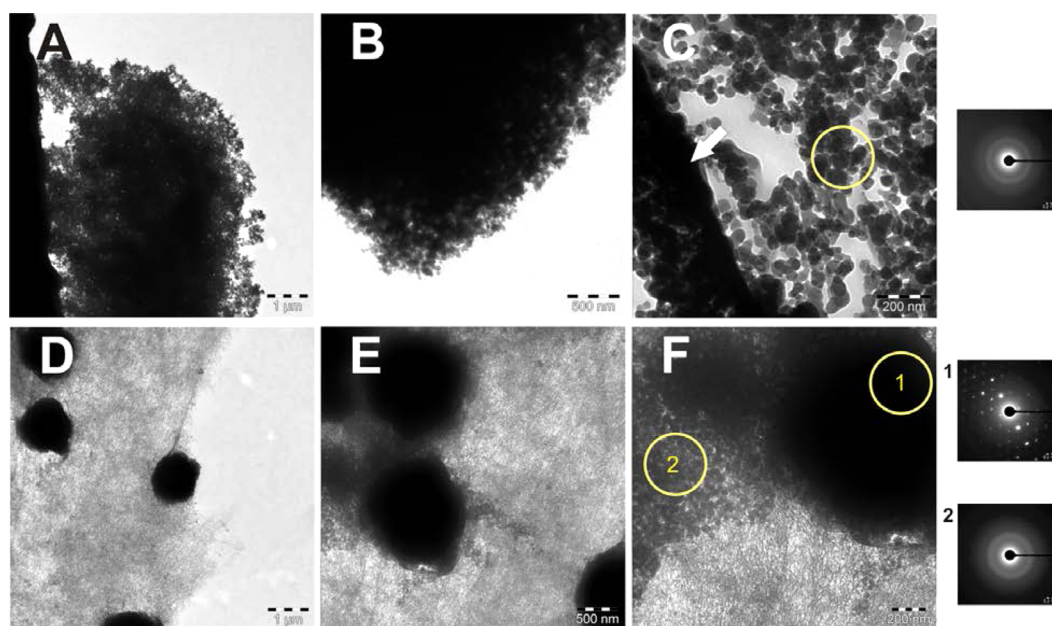


**Figure 4.** TEM images of products nucleated in the presence of low viscosity alginate (40 mg/L) at (A–C) pH 9.0 and (D–F) 9.75. SAED patterns correspond to the regions shown in C and F.

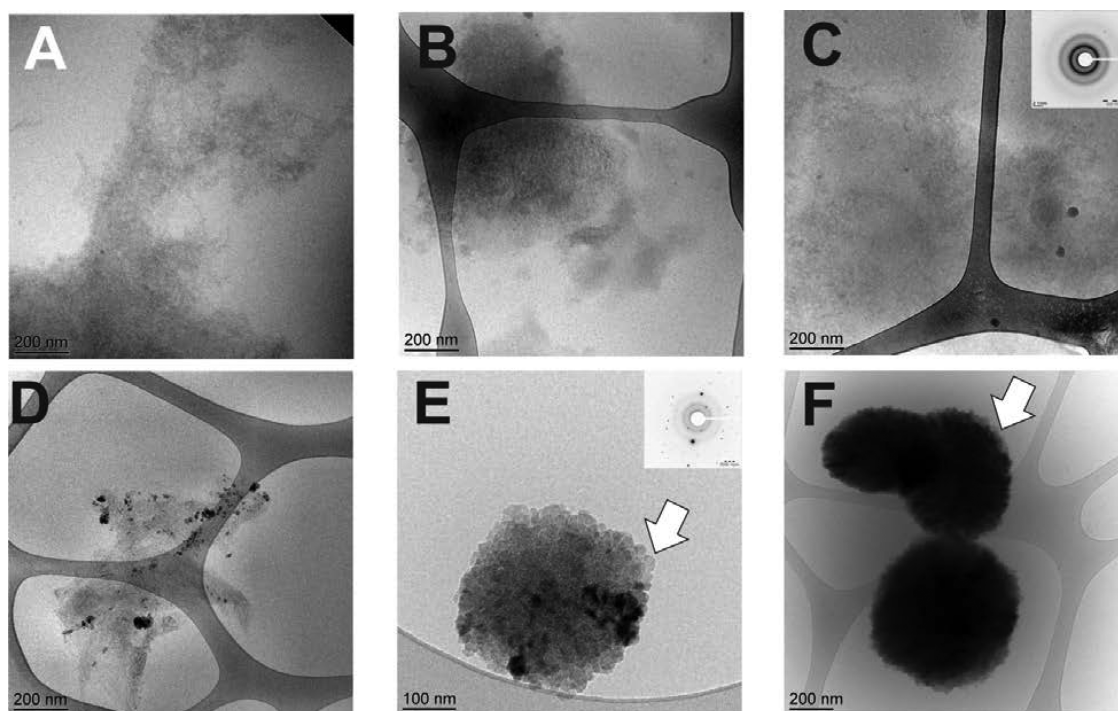


**Figure 5.** Cryo-TEM images of samples taken during progression of titrations containing low viscosity alginate (40 mg/L) at pH 9.75, representing prenucleation (A–B), nucleation (C–D) and postnucleation (E–F) regimes. Scale bars represent (A–D, F) 200 nm and (E) 100 nm.

is typical of monocrystalline vaterite with reflections at  $d$  values of 3.64 and 4.46 Å corresponding to the {110} and {014} faces (Figure 5E), respectively. This pattern can be indexed as a hexagonal vaterite  $\text{CaCO}_3$  viewed from the (001) zone axis by using JEMS crystallography software (Figure S11). Thus, the high-energy vaterite (001) surface is stabilized by the adsorption of alginate additives.<sup>63</sup> Similar structures are reported for gas diffusion assays in the presence of a chemical derivative of cellulose, a ubiquitous polysaccharide.<sup>38</sup> Since the individual constituent nanoparticles are crystallographically,

mutually oriented (arrow, Figure 5E), these structures are mesocrystalline.<sup>64</sup> The self-assembly properties of alginate molecules thus affect transient mineralization precursors and further mediate the formation of  $\text{CaCO}_3$  superstructures. These effects might be on account of synergistic interactions between the egg-box molecular structure of alginate assemblies<sup>31</sup> and the mineral precursors. The egg box model shows that the complexation of  $\text{Ca}^{2+}$  ion to the G units leads to their self-association of these units in alginate molecules. This can lead to the formation of local sites enriched in  $\text{Ca}^{2+}$  ions. In the

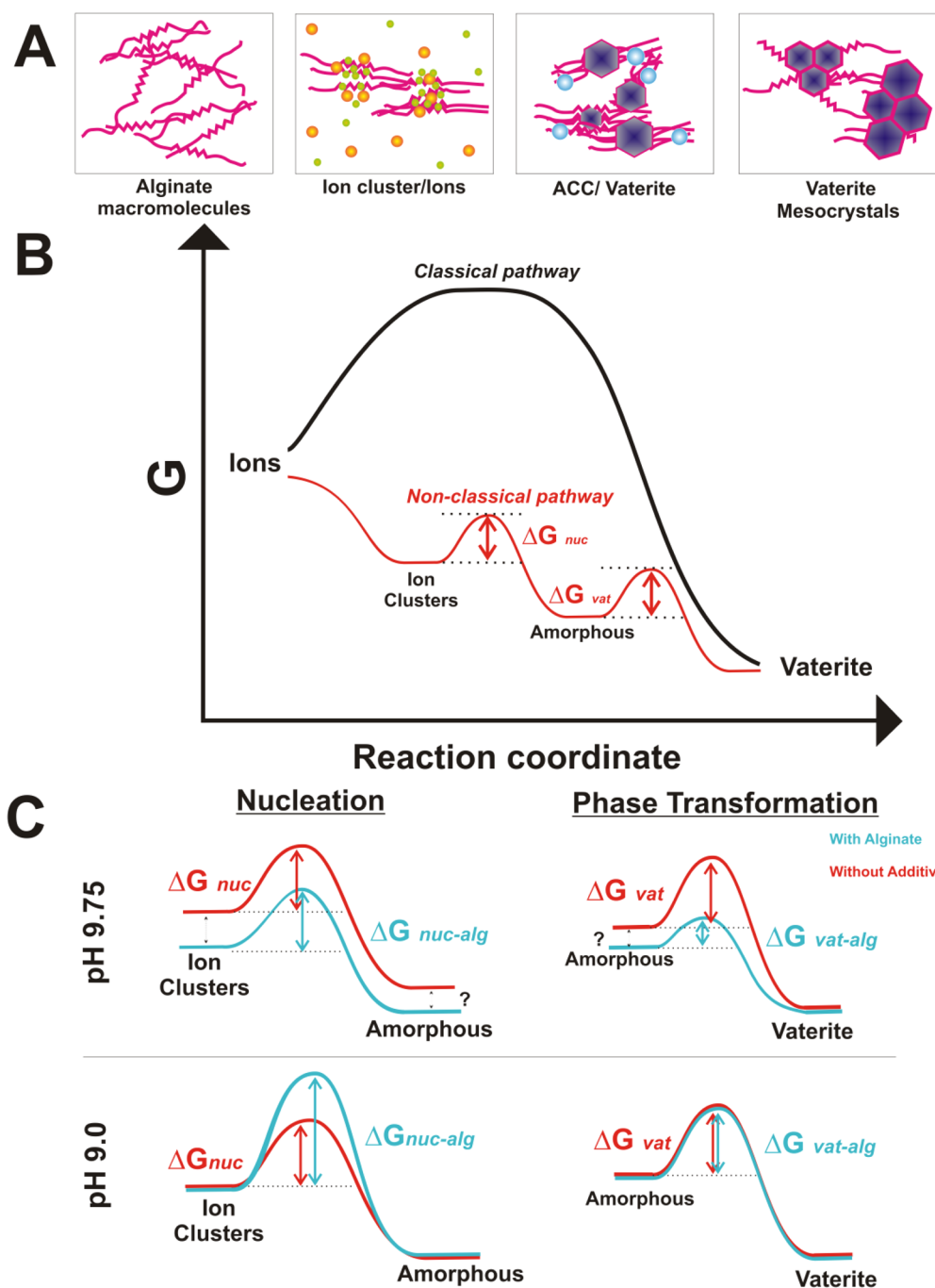


**Figure 6.** (A) Representation of mineralization in the presence of alginate molecules via their interactions with ion clusters, amorphous species, and crystalline particles (see text for explanation). Schematics depicting the free energy variation for nucleation and crystallization (B) according to the notions of the prenucleation cluster pathway (red) and direct nucleation of vaterite according to classical nucleation theory (black). Note that the stability of the amorphous intermediate, namely, proto-calcite and proto-vaterite at pH 9.0 and pH 9.75, respectively, varies in a pH-dependent manner (not shown). (C) At pH 9.75, the presence of alginates initially leads to formation of more stable calcium carbonate clusters and promotes the precipitation of vaterite from a short-lived amorphous phase; however, our data do not reveal whether or not the amorphous intermediate is thermodynamically stabilized (as indicated by the question mark) or destabilized. The free energy barrier associated with vaterite formation is lower in the presence of alginates ( $\Delta G_{vat-alg} < \Delta G_{vat}$ ). At pH 9.0, in the presence of alginates (blue curve), nucleation is inhibited ( $\Delta G_{nuc} < \Delta G_{nuc-alg}$ ), and the phase transformation of amorphous precursors is not significantly affected.

presence of excess carbonate ion species, these local sites can potentially serve as space-limited nucleation sites on account of the  $\text{Ca}^{2+}$  induced association of G units in the alginate gel matrix (Figure 6A). This is supported by enhanced assembly states of alginate molecules under conditions of nucleation and mineral growth (Figure S12). In water,  $\text{Ca}^{2+}$  induced alginate aggregation leads to species with sedimentation coefficients of

about 4.9 S, 9.1 S, 13.1 S, and 18.5 S, with the smallest species being the most abundant (about 81.5%, as calculated from Gaussian fits of the peaks). However, when in carbonate buffer,  $\text{Ca}^{2+}$  ions lead to a large distribution with species corresponding to 2.1 S, 10.1 S, 16.9 S, 22.2 S, 31.5 S, and 53.4 S. Here the 2.1 and 53.4 S species are more abundant corresponding to 56.4% and 24.4%, respectively.

**Crystallization.** To investigate the role of alginates on final crystal morphology, we also performed gas diffusion assays in the presence of these additives (Figure S13). Commercial low viscosity alginate and alginate from *L. trabeculata* lead to calcite particles with rounded edges. However, commercial medium viscosity alginate and that isolated from *L. nigrescens* lead to the formation of particles with spherical and complex morphologies suggestive of vaterite. Considering that different crystal morphologies emerge in the presence of these alginate samples, it follows that although members of certain additive classes can induce similar effects on the nucleation regime, their effects on crystal growth and formation can significantly differ. To further understand the emergence of such effects, chemical properties such as M/G ratio and physical properties such as viscosity (determined by its molar mass as given by the MHKS equation) of commercial alginates can be taken into account. <sup>1</sup>H NMR studies have shown the M/G ratio of low and medium viscosity commercial alginate to be 1.5 and 1.6, respectively.<sup>65</sup> The Brookfield viscosity (supplier provided) of low and medium viscosity alginates are about 100–300 cps and ~2000 cps, respectively. Here the role of alginates in determining final crystal morphology appears to be primarily affected by viscosity of alginates, i.e., their molar mass. Crystal morphologies similar to calcite rhombohedra are more prevalent in the presence of low viscosity commercial alginates. Commercial alginates with higher viscosity lead to spherical particles and appear to deviate from the thermodynamically stable morphologies.

**From Nucleation to Crystallization.** In the present study, alginate additives modify CaCO<sub>3</sub> crystallization pathways during which crystalline phases are the preferred nucleation products at higher pH values. The stabilities of CaCO<sub>3</sub> prenucleation clusters affect the solubility products of the phases formed after nucleation (Figure 6B,C). Alginate containing potentiometric titrations performed at pH 9.75 exhibit decreased prenucleation slopes and the formation of vaterite after nucleation. Thus, prenucleation stages of mineralization processes are significant in determining the composition of mineral products and can contribute to polymorph selectivity.<sup>19</sup> Recent reports suggest that Ca<sup>2+</sup> binding properties of certain polyelectrolytes play a key role in biomineralization during which local supersaturation determines mineral formation.<sup>66–70</sup> However, in the present study by using a Ca<sup>2+</sup> binding biopolymer, i.e., alginate, we observe distinct effects on mineralization at pH 9.0 and 9.75. This cannot be explained by local supersaturation alone. First, considering the organic phase, i.e., alginate molecules, a change of ΔpH 0.75 in the range of pH 9.0 will not significantly affect the dissociation state of carboxylate groups in the alginate sugar residues. It follows that the pH dependence of nucleation in the presence of alginates cannot be solely attributed to ion-binding since in the egg-box model alginate structuration applies to both pH values. Alternatively mineral precursors such as PNCs and amorphous phases are more responsive to changes in pH in terms of composition, size, and proto-structure.<sup>51,71</sup> This indicates the prevalence of diverse mineralization pathways.<sup>44</sup> Results of electron microscopy for samples synthesized at pH 9.75 also indicate that ACC precedes the formation of vaterite. However, the evasion of this phase, i.e., low solubilities noted after nucleation ( $<3 \times 10^{-8} \text{ M}^2$ ) in corresponding potentiometric titration data, indicates that this amorphous phase is transient (Figure 6C). Note that the solubility products observed in the above-described titration experiments corre-

spond to the most soluble products. Solubility products corresponding to vaterite ( $<3 \times 10^{-8} \text{ M}^2$ ) indicate that alginate assemblies “actively” promote the transformation of mineral precursors to crystalline phases. Nucleation products in corresponding reference experiments exhibit a solubility product of about  $3.6 \times 10^{-8} \text{ M}^2$  suggestive of amorphous phases. This is also consistent with a previous study where ACC is formed in the presence of alginates.<sup>62</sup> This study also proposed a formation mechanism for the lens-like structures in which the Ca<sup>2+</sup>-alginate interactions induce certain proto-structure in ACC and also further “partially oriented aggregation” of the ACC particles.<sup>62</sup> Here our titration assays and FTIR analyses show that vateritic proto-structuring maybe a prerequisite for the formation of the vateritic mesocrystalline superstructures. Second, the physical association of ACC and vaterite particles with alginate assemblies indicates the role of alginate in promoting phase transformation as well as particle assembly. At present, the exact mechanism of the phase transformation involved is difficult to address. Also our observations are consistent with the Oswald-Lussac law, which states that phase transformations proceed along a series of increasingly stable intermediate phases and depend on the solubilities of the phases and on the free energies of activation.<sup>2,72</sup> An alternative explanation for vaterite formation would be the kinetic precipitation of vaterite in the presence of alginates. However, this does not account for the pH-dependent behavior of alginates that leads to vaterite formation from transient ACC at higher pH values. This hints toward the role of PNCs and proto-structures in amorphous intermediates in phase transformation and thus polymorph selection (Figure 6B). In the literature, the role of particle fusion and Oswald ripening has been suggested.<sup>62</sup> This agrees with the nonclassical route of crystal growth wherein precursor nanoparticles can attach in an iso-oriented manner to form larger crystals.<sup>44</sup> In the present study, the formation of vateritic superstructures could also be a consequence of oriented attachment to primary vaterite nanoparticles. This might contribute to phase transformation observed here. Furthermore, alginate additives can bind to vaterite crystals<sup>36</sup> serving as a “capping agent” to stabilize the individual nanoparticles (Figure 6A). This growth model fits well with the descriptions of nonclassical crystallization which also encompasses the recently reported “particle accretion growth mechanism”.<sup>44,73,74</sup> Considering the effect of alginates on crystal growth, the different morphologies observed can be a consequence of the differences in chemical configuration specifically the M/G ratio and physical properties such as the resulting solution viscosity. However, it is evident from gas diffusion studies that crystal shapes are highly affected by additive solution viscosity. Such structure–function relationships are also evident in the prenucleation regime wherein a more pronounced inhibition of nucleation is found in the presence of low viscosity commercial alginate in comparison to the medium viscosity alginate. This can be attributed to (i) a higher content of L-gulonate residues that are involved in ion complexation and (ii) a lower solution viscosity and better diffusion in comparison to medium viscosity alginate containing mixtures.

In summary, our results agree well with the nonclassical concept of nucleation and crystallization that addresses the role of PNCs in crystal nucleation and growth.<sup>15,18</sup> The stabilities of CaCO<sub>3</sub> PNCs certainly affect the solubility products of the phases formed postnucleation (Figure 6B,C). This observation has been noted earlier in context of the pH dependence for

different ACC proto-structures.<sup>19,51</sup> However, in the recent studies, additive-mediated changes in the stability of PNCs also appear to affect the products formed postnucleation.<sup>23,53</sup> Results discussed here show that solution pH is a primary determinant of organic–inorganic interactions and thus final mineral composition and structure. In nature, these interactions and their consequences on final mineral structures thus appear crucial and hence need further investigations.

The consistency of potentiometric titration assays with electron microscopy and FTIR analyses reflects that this is a reliable technique providing quantitative information about nucleation events in bulk volumes under near physiological conditions. In contrast, gas diffusion assays give qualitative evidence of additive mediated changes in crystal morphology, polymorphism, or crystallization mechanism and do not reveal the prenucleation stages of crystallization that the additives act upon. Another disadvantage of this assay is the lack of control over reaction pH and the presence of  $\text{NH}_4^+$  ions that drastically affect the structural integrity of certain biomolecules,<sup>74</sup> but can also act as an additive as such which can influence the mineralization reaction of  $\text{CaCO}_3$ .<sup>76</sup> For a better understanding of mineralization phenomena, complementary techniques that probe bulk properties in a quantitative manner are essential.

## CONCLUSIONS

The present study shows that solution pH is a critical factor that affects the interactions between mineralization additives and transient inorganic phases and in turn determines the properties of subsequent mineral products such as composition and structure. Such observations cannot be satisfactorily described by classical crystal growth models that describe crystal growth by ion attachment and unit cell replication.<sup>77</sup> This study also shows that prenucleation stages have an effect on postnucleation events such as nucleation of favored polymorphs. Previous titration-based studies conducted at constant pH 9.75 have shown that molecular configuration, stereochemistry, and type of molecular linkages significantly affect mineralization.<sup>23</sup> Considering the distinct pH-dependent effects observed here, the interactions between biomolecules and transient mineral species appear more complex. In addition to the biochemical properties of molecules, which are generally focused upon, the value of pH, a physiochemically fundamental parameter significantly alters on the scheme of  $\text{CaCO}_3$  mineralization. In nature, the pH-dependent modulation of biomineralization pathways has been documented. For instance, pH is a fine-tuned parameter for calcite deposition in certain foraminifera<sup>78</sup> and during avian egg-shell formation.<sup>79</sup> The consequences for such constant pH environments not only encompass the stability and structure of inorganic precursors but also their specific interactions with mineralization additives. Such interactions are possibly linked to the distinct proto-structures of PNCs and ACC<sup>51</sup> wherein certain proto-structures might be structurally more conducive for interactions with additives. To understand this, further insights into the molecular interactions between additives and mineral precursors are required.

## ASSOCIATED CONTENT

### Supporting Information

The Supporting Information is available free of charge on the ACS Publications website at DOI: 10.1021/acs.cgd.5b01488.

(1) Analytical ultracentrifugation derived sedimentation coefficient distributions for alginates in the absence and presence of  $\text{Ca}^{2+}$  ions. (2) Time development of free  $\text{Ca}^{2+}$  ions and calcium carbonate solubility products at pH 9.0 and 9.75 for titration experiments. (3) Quantitative energy-dispersive X-ray spectroscopy (EDS) and elemental mapping for mineralized samples. (4) SEM and TEM of alginates in absence of mineralization. (5) FTIR spectra of samples nucleated in the absence and presence of alginates at different pH values. (6) SEM images of particles formed using gas diffusion methodology (PDF)

## AUTHOR INFORMATION

### Corresponding Authors

\*(A.N.-C.) E-mail: [aneira@uchile.cl](mailto:aneira@uchile.cl).

\*(H.C.) E-mail: [helmut.coelfen@uni-konstanz.de](mailto:helmut.coelfen@uni-konstanz.de).

### Notes

The authors declare no competing financial interest.

## ACKNOWLEDGMENTS

This work was supported by Projects FONDECYT 1120172 and 1140660, granted by the Chilean Council for Science and Technology (CONICYT), and Project PCC12-039 CONICYT/DAAD and PCC12-038 CONICYT/MinCyt. A.N.C. is grateful for funding by Program U-Redes, Vice-presidency of Research and Development, University of Chile. P.V.-Q. acknowledges a fellowship provided by CONICYT and German Academic Exchange Service (DAAD). The authors acknowledge the funding by DAAD from the ALECHILE program for 2013/2014. A.R. acknowledges a fellowship from Konstanz Research School Chemical Biology. D.G. is a Research Fellow of the Zukunftskolleg of the University of Konstanz. We thank Dr. Roland Kröger, Department of Physics, University of York, UK, for his expert advice on analyses of electron microscopy data.

## REFERENCES

- (1) Olszta, M. J.; Cheng, X.; Jee, S. S.; Kumar, R.; Kim, Y.-Y.; Kaufman, M. J.; Douglas, E. P.; Gower, L. B. Bone structure and formation: a new perspective. *Mater. Sci. Eng., R* **2007**, *58*, 77–116.
- (2) Mann, S. *Biomineralization*; Oxford University Press: Oxford, 2001.
- (3) Politi, Y.; Arad, T.; Klein, E.; Weiner, S.; Addadi, L. Sea urchin spine calcite forms via a transient amorphous calcium carbonate phase. *Science* **2004**, *306*, 1161–1164.
- (4) Cölfen, H. Biomineralization: a crystal-clear view. *Nat. Mater.* **2010**, *9*, 960–961.
- (5) Addadi, L.; Raz, S.; Weiner, S. Taking advantage of disorder: amorphous calcium carbonate and its roles in biomineralization. *Adv. Mater.* **2003**, *15*, 959–970.
- (6) Arias, J. L.; Fernández, M. a. S. Polysaccharides and proteoglycans in calcium carbonate-based biomineralization. *Chem. Rev.* **2008**, *108*, 4475–4482.
- (7) Fernández, M. S.; Bustos, C.; Luquet, G.; Saez, D.; Neira-Carrillo, A.; Corneillat, M.; Alcaraz, G.; Arias, J. L. Proteoglycan occurrence in gastrolith of the crayfish *Cherax quadricarinatus* (Malacostraca: Decapoda). *J. Crustacean Biol.* **2012**, *32*, 802–815.
- (8) Fernandez, M. S.; Araya, M.; Arias, J. L. Eggshells are shaped by a precise spatio-temporal arrangement of sequentially deposited macromolecules. *Matrix Biol.* **1997**, *16*, 13–20.
- (9) Soledad Fernandez, M. S.; Moya, A.; Lopez, L.; Arias, J. L. Secretion pattern, ultrastructural localization and function of

extracellular matrix molecules involved in eggshell formation. *Matrix Biol.* **2001**, *19*, 793–803.

(10) Wise, E. R.; Maltsev, S.; Davies, M. E.; Duer, M. J.; Jaeger, C.; Loveridge, N.; Murray, R. C.; Reid, D. G. The organic-mineral interface in bone is predominantly polysaccharide. *Chem. Mater.* **2007**, *19*, 5055–5057.

(11) Duchstein, P.; Kniep, R.; Zahn, D. On the Function of Saccharides during the Nucleation of Calcium Carbonate-Protein Biocomposites. *Cryst. Growth Des.* **2013**, *13*, 4885–4889.

(12) Nielsen, J. W.; Sand, K. K.; Pedersen, C. S.; Lakshatnov, L. Z.; Winther, J. R.; Willemoës, M.; Stipp, S. L. S. Polysaccharide Effects on Calcite Growth: The Influence of Composition and Branching. *Cryst. Growth Des.* **2012**, *12*, 4906–4910.

(13) Yang, M.; Stipp, S. L. S.; Harding, J. Biological Control on Calcite Crystallization by Polysaccharides. *Cryst. Growth Des.* **2008**, *8*, 4066–4074.

(14) Gebauer, D.; Cölfen, H. Prenucleation clusters and non-classical nucleation. *Nano Today* **2011**, *6*, 564–584.

(15) Gebauer, D.; Kellermeier, M.; Gale, J. D.; Bergstrom, L.; Colfen, H. Pre-nucleation clusters as solute precursors in crystallisation. *Chem. Soc. Rev.* **2014**, *43*, 2348–2371.

(16) Verch, A.; Gebauer, D.; Antonietti, M.; Cölfen, H. How to control the scaling of CaCO<sub>3</sub>: a “fingerprinting technique” to classify additives. *Phys. Chem. Phys.* **2011**, *13*, 16811–16820.

(17) Dey, A.; Bomans, P. H.; Müller, F. A.; Will, J.; Frederik, P. M.; de With, G.; Sommerdijk, N. A. The role of prenucleation clusters in surface-induced calcium phosphate crystallization. *Nat. Mater.* **2010**, *9*, 1010–1014.

(18) Gebauer, D.; Völkel, A.; Cölfen, H. Stable prenucleation calcium carbonate clusters. *Science* **2008**, *322*, 1819–1822.

(19) Cartwright, J. H.; Checa, A. G.; Gale, J. D.; Gebauer, D.; Sainz-Diaz, C. I. Calcium carbonate polymorphism and its role in biomineralization: how many amorphous calcium carbonates are there? *Angew. Chem., Int. Ed.* **2012**, *51*, 11960–11970.

(20) Politi, Y.; Metzler, R. A.; Abrecht, M.; Gilbert, B.; Wilt, F. H.; Sagi, I.; Addadi, L.; Weiner, S.; Gilbert, P. Transformation mechanism of amorphous calcium carbonate into calcite in the sea urchin larval spicule. *Proc. Natl. Acad. Sci. U. S. A.* **2008**, *105*, 17362–17366.

(21) Weiss, I. M.; Tuross, N.; Addadi, L.; Weiner, S. Mollusc larval shell formation: amorphous calcium carbonate is a precursor phase for aragonite. *J. Exp. Zool.* **2002**, *293*, 478–491.

(22) Nassif, N.; Pinna, N.; Gehrke, N.; Antonietti, M.; Jäger, C.; Cölfen, H. Amorphous layer around aragonite platelets in nacre. *Proc. Natl. Acad. Sci. U. S. A.* **2005**, *102*, 12653–12655.

(23) Rao, A.; Berg, J. K.; Kellermeier, M.; Gebauer, D. Sweet on biomineralization: effects of carbohydrates on the early stages of calcium carbonate crystallization. *Eur. J. Mineral.* **2014**, *26*, 537–552.

(24) Kloareg, B.; Quatrano, R. Structure of the cell walls of marine algae and ecophysiological functions of the matrix polysaccharides. *Oceanogr. Mar. Biol.* **1988**, *26*, 259–315.

(25) Haug, A.; Larsen, B.; Smidsrød, O. Uronic acid sequence in alginate from different sources. *Carbohydr. Res.* **1974**, *32*, 217–225.

(26) Craigie, J.; Morris, E.; Rees, D.; Thom, D. Alginate block structure in Phaeophyceae from Nova Scotia: variation with species, environment and tissue-type. *Carbohydr. Polym.* **1984**, *4*, 237–252.

(27) Smidsrød, O. Molecular basis for some physical properties of alginates in the gel state. *Faraday Discuss. Chem. Soc.* **1974**, *57*, 263–274.

(28) Grant, G. T.; Morris, E. R.; Rees, D. A.; Smith, P. J.; Thom, D. Biological interactions between polysaccharides and divalent cations: the egg-box model. *FEBS Lett.* **1973**, *32*, 195–198.

(29) Braccini, I.; Pérez, S. Molecular basis of Ca<sup>2+</sup>-induced gelation in alginates and pectins: the egg-box model revisited. *Biomacromolecules* **2001**, *2*, 1089–1096.

(30) Sikorski, P.; Mo, F.; Skjåk-Bræk, G.; Stokke, B. T. Evidence for Egg-Box-Compatible Interactions in Calcium-Alginate Gels from Fiber X-ray Diffraction. *Biomacromolecules* **2007**, *8*, 2098–2103.

(31) Fang, Y.; Al-Assaf, S.; Phillips, G. O.; Nishinari, K.; Funami, T.; Williams, P. A.; Li, L. Multiple steps and critical behaviors of the binding of calcium to alginate. *J. Phys. Chem. B* **2007**, *111*, 2456–2462.

(32) Li, L.; Fang, Y.; Vreeker, R.; Appelqvist, I.; Mendes, E. Reexamining the Egg-Box Model in Calcium-Alginate Gels with X-ray Diffraction. *Biomacromolecules* **2007**, *8*, 464–468.

(33) Addadi, L.; Joester, D.; Nudelman, F.; Weiner, S. Mollusk shell formation: a source of new concepts for understanding biomineralization processes. *Chem.—Eur. J.* **2006**, *12*, 980–987.

(34) Li, H.; Xin, H. L.; Muller, D. A.; Estroff, L. A. Visualizing the 3D internal structure of calcite single crystals grown in agarose hydrogels. *Science* **2009**, *326*, 1244–1247.

(35) Salgado, L. T.; Amado Filho, G. M.; Fernandez, M. S.; Arias, J. L.; Farina, M. The effect of alginates, fucans and phenolic substances from the brown seaweed *Padina gymnospora* in calcium carbonate mineralization in vitro. *J. Cryst. Growth* **2011**, *321*, 65–71.

(36) Olderøy, M. Ø.; Xie, M.; Strand, B. L.; Flaten, E. M.; Sikorski, P.; Andreassen, J.-P. Growth and Nucleation of Calcium Carbonate Vaterite Crystals in Presence of Alginate. *Cryst. Growth Des.* **2009**, *9*, 5176–5183.

(37) Cölfen, H.; Antonietti, M. Crystal Design of Calcium Carbonate Microparticles Using Double-Hydrophilic Block Copolymers. *Langmuir* **1998**, *14*, 582–589.

(38) Cölfen, H. Double-Hydrophilic Block Copolymers: Synthesis and Application as Novel Surfactants and Crystal Growth Modifiers. *Macromol. Rapid Commun.* **2001**, *22*, 219–252.

(39) Yu, S.-H.; Antonietti, M.; Cölfen, H.; Hartmann, J. Growth and self-assembly of BaCrO<sub>4</sub> and BaSO<sub>4</sub> nanofibers toward hierarchical and repetitive superstructures by polymer-controlled mineralization reactions. *Nano Lett.* **2003**, *3*, 379–382.

(40) Cölfen, H.; Qi, L. A Systematic Examination of the Morphogenesis of Calcium Carbonate in the Presence of a Double-Hydrophilic Block Copolymer. *Chem. - Eur. J.* **2001**, *7*, 106–116.

(41) Spiro, T. G.; Allerton, S. E.; Renner, J.; Terzis, A.; Bils, R.; Saltman, P. The Hydrolytic Polymerization of Iron(III). *J. Am. Chem. Soc.* **1966**, *88*, 2721–2726.

(42) Gebauer, D.; Cölfen, H.; Verch, A.; Antonietti, M. The multiple roles of additives in CaCO<sub>3</sub> crystallization: A quantitative case study. *Adv. Mater.* **2009**, *21*, 435–439.

(43) Nudelman, F.; Pieterse, K.; George, A.; Bomans, P. H. H.; Friedrich, H.; Brylka, L. J.; Hilbers, P. A. J.; de With, G.; Sommerdijk, N. A. J. M. The role of collagen in bone apatite formation in the presence of hydroxyapatite nucleation inhibitors. *Nat. Mater.* **2010**, *9*, 1004–1009.

(44) Niederberger, M.; Cölfen, H. Oriented attachment and mesocrystals: non-classical crystallization mechanisms based on nanoparticle assembly. *Phys. Chem. Chem. Phys.* **2006**, *8*, 3271–3287.

(45) Kellermeier, M.; Picker, A.; Kempter, A.; Cölfen, H.; Gebauer, D. A Straightforward Treatment of Activity in Aqueous CaCO<sub>3</sub> Solutions and the Consequences for Nucleation Theory. *Adv. Mater.* **2014**, *26*, 752–757.

(46) Brečević, L.; Nielsen, A. E. Solubility of amorphous calcium carbonate. *J. Cryst. Growth* **1989**, *98*, 504–510.

(47) Ogino, T.; Suzuki, T.; Sawada, K. The formation and transformation mechanism of calcium carbonate in water. *Geochim. Cosmochim. Acta* **1987**, *51*, 2757–2767.

(48) Gomez, C. G.; Pérez Lambrecht, M. V.; Lozano, J. E.; Rinaudo, M.; Villar, M. A. Influence of the extraction-purification conditions on final properties of alginates obtained from brown algae (*Macrocystis pyrifera*). *Int. J. Biol. Macromol.* **2009**, *44*, 365–371.

(49) Schuck, P. Size-distribution analysis of macromolecules by sedimentation velocity ultracentrifugation and lamm equation modeling. *Biophys. J.* **2000**, *78*, 1606–1619.

(50) Kellermeier, M.; Cölfen, H.; Gebauer, D. Investigating the Early Stages of Mineral Precipitation by Potentiometric Titration and Analytical Ultracentrifugation. *Methods Enzymol.* **2013**, *532*, 45–69.

(51) Gebauer, D.; Gunawidjaja, P. N.; Ko, J.; Bacsik, Z.; Aziz, B.; Liu, L.; Hu, Y.; Bergström, L.; Tai, C. W.; Sham, T. K.; et al. Proto-Calcite

and Proto-Vaterite in Amorphous Calcium Carbonates. *Angew. Chem.* **2010**, *122*, 9073–9075.

(52) Neira-Carrillo, A.; Vásquez-Quitral, P.; Paz Díaz, M.; Soledad Fernández, M.; Luis Arias, J.; Yazdani-Pedram, M. Control of calcium carbonate crystallization by using anionic polymethylsiloxanes as templates. *J. Solid State Chem.* **2012**, *194*, 400–408.

(53) Picker, A.; Kellermeier, M.; Seto, J.; Gebauer, D.; Cölfen, H. The multiple effects of amino acids on the early stages of calcium carbonate crystallization. *Z. Kristallogr. - Cryst. Mater.* **2012**, *227*, 744–757.

(54) Wang, S.-S.; Picker, A.; Cölfen, H.; Xu, A.-W. Heterostructured calcium carbonate microspheres with calcite equatorial loops and vaterite spherical cores. *Angew. Chem., Int. Ed.* **2013**, *52*, 6317–6321.

(55) Rao, A.; Seto, J.; Berg, J. K.; Kreft, S. G.; Scheffner, M.; Cölfen, H. Roles of larval sea urchin spicule SMSO domains in organic matrix self-assembly and calcium carbonate mineralization. *J. Struct. Biol.* **2013**, *183*, 205–215.

(56) Perovic, I.; Chang, E. P.; Lui, M.; Rao, A.; Cölfen, H.; Evans, J. S. A nacre protein, n16. 3, self-assembles to form protein oligomers that dimensionally limit and organize mineral deposits. *Biochemistry* **2014**, *53*, 2739–2748.

(57) Perovic, I.; Verch, A.; Chang, E. P.; Rao, A.; Cölfen, H.; Kröger, R.; Evans, J. S. An Oligomeric C-RING Nacre Protein Influences Prenucleation Events and Organizes Mineral Nanoparticles. *Biochemistry* **2014**, *53*, 7259–7268.

(58) Eiblmeier, J.; Schurmann, U.; Kienle, L.; Gebauer, D.; Kunz, W.; Kellermeier, M. New insights into the early stages of silica-controlled barium carbonate crystallization. *Nanoscale* **2014**, *6*, 14939–14949.

(59) Draget, K. I.; Skjåk Bræk, G.; Smidsrød, O. Alginic acid gels: the effect of alginate chemical composition and molecular weight. *Carbohydr. Polym.* **1994**, *25*, 31–38.

(60) Hayzelden, C.; Batstone, J.; Cammarata, R. In situ transmission electron microscopy studies of silicide-mediated crystallization of amorphous silicon. *Appl. Phys. Lett.* **1992**, *60*, 225–227.

(61) Bewernitz, M. A.; Gebauer, D.; Long, J.; Cölfen, H.; Gower, L. B. A metastable liquid precursor phase of calcium carbonate and its interactions with polyaspartate. *Faraday Discuss.* **2012**, *159*, 291–312.

(62) Leng, B.; Jiang, F.; Lu, K.; Ming, W.; Shao, Z. Growth of calcium carbonate mediated by slowly released alginate. *CrystEngComm* **2010**, *12*, 730–736.

(63) Xu, A. W.; Antonietti, M.; Cölfen, H.; Fang, Y. P. Uniform Hexagonal Plates of Vaterite CaCO<sub>3</sub> Mesocrystals Formed by Biomimetic Mineralization. *Adv. Funct. Mater.* **2006**, *16*, 903–908.

(64) Bergström, L.; Sturm, E. V.; Salazar-Alvarez, G.; Cölfen, H. Mesocrystals in Biominerals and Colloidal Arrays. *Acc. Chem. Res.* **2015**, *48*, 1391–1402.

(65) Lawrie, G.; Keen, I.; Drew, B.; Chandler-Temple, A.; Rintoul, L.; Fredericks, P.; Grøndahl, L. Interactions between alginate and chitosan biopolymers characterized using FTIR and XPS. *Biomacromolecules* **2007**, *8*, 2533–2541.

(66) Wang, T.; Cölfen, H.; Antonietti, M. Nonclassical Crystallization: Mesocrystals and Morphology Change of CaCO<sub>3</sub> Crystals in the Presence of a Polyelectrolyte Additive. *J. Am. Chem. Soc.* **2005**, *127*, 3246–3247.

(67) Meldrum, F. C.; Cölfen, H. Controlling mineral morphologies and structures in biological and synthetic systems. *Chem. Rev.* **2008**, *108*, 4332–4432.

(68) Tong, H.; Ma, W.; Wang, L.; Wan, P.; Hu, J.; Cao, L. Control over the crystal phase, shape, size and aggregation of calcium carbonate via a L-aspartic acid inducing process. *Biomaterials* **2004**, *25*, 3923–3929.

(69) Smeets, P. J. M.; Cho, K. R.; Kempen, R. G. E.; Sommerdijk, N. A. J. M.; De Yoreo, J. J. Calcium carbonate nucleation driven by ion binding in a biomimetic matrix revealed by in situ electron microscopy. *Nat. Mater.* **2015**, *14*, 394–399.

(70) Addadi, L.; Moradian, J.; Shay, E.; Maroudas, N.; Weiner, S. A chemical model for the cooperation of sulfates and carboxylates in calcite crystal nucleation: relevance to biomineralization. *Proc. Natl. Acad. Sci. U. S. A.* **1987**, *84*, 2732–2736.

(71) Koga, N.; Nakagoe, Y.; Tanaka, H. Crystallization of amorphous calcium carbonate. *Thermochim. Acta* **1998**, *318*, 239–244.

(72) Cölfen, H.; Mann, S. Higher-Order Organization by Mesoscale Self-Assembly and Transformation of Hybrid Nanostructures. *Angew. Chem., Int. Ed.* **2003**, *42*, 2350–2365.

(73) Gal, A.; Kahil, K.; Vidavsky, N.; DeVol, R. T.; Gilbert, P. U. P. A.; Fratzl, P.; Weiner, S.; Addadi, L. Particle Accretion Mechanism Underlies Biological Crystal Growth from an Amorphous Precursor Phase. *Adv. Funct. Mater.* **2014**, *24*, 5420–5426.

(74) De Yoreo, J. J.; Gilbert, P. U.; Sommerdijk, N. A.; Penn, R. L.; Whitelam, S.; Joester, D.; Zhang, H.; Rimer, J. D.; Navrotsky, A.; Banfield, J. F.; et al. Crystallization by particle attachment in synthetic, biogenic, and geologic environments. *Science* **2015**, *349* (6247), aaa6760.

(75) Benesch, R. E.; Lardy, H. A.; Benesch, R. The sulfhydryl groups of crystalline proteins: i. some albumins, enzymes, and hemoglobins. *J. Biol. Chem.* **1955**, *216*, 663–676.

(76) Gehrke, N.; Cölfen, H.; Pinna, N.; Antonietti, M.; Nassif, N. Superstructures of calcium carbonate crystals by oriented attachment. *Cryst. Growth Des.* **2005**, *5*, 1317–1319.

(77) Kashchiev, D. *Nucleation*; Butterworth-Heinemann: Oxford, 2000.

(78) de Nooijer, L. J.; Toyofuku, T.; Kitazato, H. Foraminifera promote calcification by elevating their intracellular pH. *Proc. Natl. Acad. Sci. U. S. A.* **2009**, *106*, 15374–15378.

(79) Hodges, R. D. pH and mineral ion levels in the blood of the laying hen (*Gallus domesticus*) in relation to egg shell formation. *Comp. Biochem. Physiol.* **1969**, *28*, 1243–1257.